HHS Public Access

Author manuscript

*Adv Funct Mater*. Author manuscript; available in PMC 2021 September 15.

Published in final edited form as:

*Adv Funct Mater*. 2018 October 10; 28(41): . doi:10.1002/adfm.201804076.

# Cyclodextrin Modulated Type I Collagen Self-Assembly to Engineer Biomimetic Cornea Implants

**Shoumyo Majumdar**,
Translational Tissue Engineering Center, Johns Hopkins University, Baltimore, MD 21231, USA

Department of Materials Science and Engineering, Johns Hopkins University, Baltimore, MD 21218, USA

Department of Biomedical Engineering, Johns Hopkins University, Baltimore, MD 21218, USA

**Xiaokun Wang**,
Translational Tissue Engineering Center, Johns Hopkins University, Baltimore, MD 21231, USA

Department of Biomedical Engineering, Johns Hopkins University, Baltimore, MD 21218, USA

Wilmer Eye Institute, Johns Hopkins School of Medicine Baltimore, MD 21231, USA

**Sven D. Sommerfeld**,
Translational Tissue Engineering Center, Johns Hopkins University, Baltimore, MD 21231, USA

Department of Biomedical Engineering, Johns Hopkins University, Baltimore, MD 21218, USA

Wilmer Eye Institute, Johns Hopkins School of Medicine Baltimore, MD 21231, USA

**Jemin Jeremy Chae**,
Translational Tissue Engineering Center, Johns Hopkins University, Baltimore, MD 21231, USA

Department of Biomedical Engineering, Johns Hopkins University, Baltimore, MD 21218, USA

Wilmer Eye Institute, Johns Hopkins School of Medicine Baltimore, MD 21231, USA

**Evangelia-Nefeli Athanasopoulou**,
Supramolecular Nanomaterials and Interfaces Laboratory, École Polytechnique Fédérale de Lausanne, Lausanne 1015, Switzerland

**Lucas S. Shores**,
Department of Biomedical Engineering, Johns Hopkins University, Baltimore, MD 21218, USA

**Xiaodong Duan**,
Eyegenix LLC, Honolulu, HI 96817, USA

**L. Mario Amzel**,

asingh29@jhu.edu .

Supporting Information
Supporting Information is available from the Wiley Online Library or from the author.

Conflict of Interest
The authors declare no conflict of interest.

Department of Biophysics and Biophysical Chemistry, Johns Hopkins University, Baltimore, MD 21205, USA

**Francesco Stellacci**,
Supramolecular Nanomaterials and Interfaces Laboratory, École Polytechnique Fédérale de Lausanne, Lausanne 1015, Switzerland

**Oliver Schein**,
Wilmer Eye Institute, Johns Hopkins School of Medicine Baltimore, MD 21231, USA

**Qiongyu Guo**,
Department of Biomedical Engineering, Johns Hopkins University, Baltimore, MD 21218, USA

Department of Biomedical Engineering, Southern University of Science and Technology, Shenzhen, Guangdong 518055, China

**Anirudha Singh**,
Translational Tissue Engineering Center, Johns Hopkins University, Baltimore, MD 21231, USA

Deparment of Urology, Johns Hopkins School of Medicine & Department of Chemical and Biomolecular Engineering, Johns Hopkins University, Baltimore, MD 21218, USA

**Jennifer H. Elisseeff**
Translational Tissue Engineering Center, Johns Hopkins University, Baltimore, MD 21231, USA

Department of Materials Science and Engineering, Johns Hopkins University, Baltimore, MD 21218, USA

Department of Biomedical Engineering, Johns Hopkins University, Baltimore, MD 21218, USA

Wilmer Eye Institute, Johns Hopkins School of Medicine Baltimore, MD 21231, USA

## Abstract

Collagen-rich tissues in the cornea exhibit unique and highly organized extracellular matrix ultrastructures, which contribute to its high load-bearing capacity and light transmittance. Corneal collagen fibrils are controlled during development by small leucine-rich proteoglycans (SLRPs) that regulate the fibril diameter and spacing in order to achieve the unique optical transparency. Cyclodextrins (CDs) of varying size and chemical functionality for their ability to regulate collagen assembly during vitrification process are screened in order to create biosynthetic materials that mimic the native cornea structure. Addition of βCD to collagen vitrigels produces materials with aligned fibers and lamellae similar to native cornea, resulting in mechanically robust and transparent materials. Biochemistry analysis revealed that CD interacts with hydrophobic amino acids in collagen to influence assembly and fibril organization. To translate the self-assembled collagen materials for cornea reconstruction, custom molds for gelation and vitrification are engineered to create βCD/Col implants with curvature matching that of the cornea. Acellular βCD/Col materials are implanted in a rabbit partial keratoplasty model with interrupted sutures. The implants demonstrate tissue integration and support re-epithelialization. Therefore, the addition of CD molecules regulates collagen self-assembly and provides a simple process to engineer corneal mimetic substitutes with advanced structural and functional properties.

**Keywords**

collagen; cornea; cyclodextrins; fibril alignment; self-assembly

## 1. Introduction

Collagen type I is the most common protein found in the body,[1] and it serves a critical role as a structural building block in many tissues. Type I Collagen triple helices can self-assemble into fibrils in a hierarchical 3D organization. Organization of collagen fibrils, such as parallel alignment, provides additional mechanisms for controlling mechanical properties impacting biological responses.[2–4] The structural features and self-assembly properties of collagen can be leveraged to create biomaterials with unique physical and biological properties for studying cell– matrix interactions and for engineering functional biomaterials.

In the cornea, collagen has a particularly unique structural and functional organization that is responsible for creating a robust, transparent tissue.[5] Collagen fibril in the cornea is ≈36 nm in diameter, which is small compared to most of the other tissues in the body, and the fibrils are aligned in parallel to form lamellae.[6] Furthermore, the parallel alignment of the collagen fibrils in each lamella runs orthogonal to adjacent layers, providing anisotropic mechanical integrity.[7] The lamellae and collagen fibrils are spaced in a highly regular arrangement, which bestows the cornea tissue unique refractive properties,[8,9] creating a transparent structure that serves as the window to the eye. The complex matrix organization in the cornea is formed during embryological development. SLRPs such as decorin, biglycan, keratocan, and lumican play critical roles in regulating and guiding the collagen fibrogenesis and spacing.[10–12]

There is a significant clinical need to create corneal substitutes as an alternative to human cadaveric transplantation. While in many respects a successful surgery, allograft corneal transplantation requires donor tissue, suffers from slow, chronic mechanical failure, and is prone to immune rejection. When transplantation fails, as in up to 70% of cases in highrisk patients with vascularization or previous transplant rejection history,[13–16] few alternatives exist today. Early attempts to create an off-the-shelf cornea substitute utilized synthetic polymers such as poly(methyl methacrylate) and poly(2-hydroxyethyl methacrylate). Cornea implants derived from these synthetic materials do not integrate with the surrounding tissue, stimulate inflammation with neovascularization, and are often ultimately extruded from the eye through a process called corneal melting.[17] More recently, biological corneal substitutes have been synthesized from collagen.[18–22] These collagen implants are more biocompatible than synthetic polymers, but generally lack structural organization, and thus, functional properties of native tissue. Without the native corneal structure, it is challenging to simultaneously achieve both the mechanical properties adequate for suturing and the transparency for vision. Methods to concentrate collagen, including vitrification, can produce orthogonal lamellae similar to the native tissue[23–27] but the materials do not reach the thickness of the human cornea relevant for clinical transplantation. While these materials may be useful as membranes for delivering cells, an off-the-shelf, acellular cornea substitute

that stimulates endogenous cells to reconstruct cornea tissues provides an alternative to cadaveric allotransplantation and injury repair.

Design requirements for cornea substitutes are unique and include transparency for vision combined with adequate mechanical integrity to support direct sutures. Here, we reported that CD were able to modulate collagen fibrogenesis and arrangement, and created a highly transparent and mechanically robust collagen vitrigel implant with a unique ultrastructure that mimics native corneas. Cyclodextrins (CD) interacted with collagen molecules during early gelation in collagen hydrogels,[28] and further in the vitrification process[29–33] to guide the fibril formation into lamellae stacks. Biocompatibility and surgical performance of the biomimetic CD/collagen implants were validated in vitro, and in a rabbit partial keratectomy cornea injury model.

## 2. Results and Discussions

### 2.1. CD Modulate Collagen Self-Assembly and Biomaterial Properties

To determine the potential use of CD to regulate collagen assembly, we screened CDs with varying size and functionality for their ability to control type I collagen self-assembly and form biomaterials with an architecture similar to the native cornea (Figure 1). CDs are circular oligosaccharides with varying internal diameter depending on the number of sugars ($\alpha$CD, $\beta$CD, $\gamma$CD) (Figure S1a, Supporting Information). The hydrophobicity of the CD interior core[34] allows the formation of complexes with hydrophobic compounds. The CD exterior is hydrophilic, and the base alcohol groups can be replaced with various functional groups such as phosphate(-$PO_4$), succinyl (abbreviated as—Suc), methyl(–$CH_3$), thiol(–SH), butyl(–$C_4H_9$), and amine (–$NH_2$). To evaluate their potential to regulate collagen assembly, these CDs were dissolved in buffer and then combined with collagen to form a gel (CD/Col) using standard conditions.[32] The CD/Col gels were subsequently vitrified, a process that provides slow, controlled dehydration under defined temperature and humidity that facilitates a gradual concentration of collagen.[35]

CD/Col materials maintained transparency when scaled up to 400 μm, close to the thickness of the human cornea. Collagen vitrigels reported in our previous study (CV, vitrified collagen gels) to serve as corneal limbal stem cell carriers[36] were under 100 μm in thickness, and they lost the transparency when the thickness was increased to that required for a corneal substitute (Figure 1b). In contrast, CD/Col materials were transparent up to the maximum tested thickness of 400 μm. In addition to clarity, the CD/Col materials had a lamellar structure similar to the native cornea (Figure 1c,d). A customized suture pull-out test (Figure 1e) found that the CD/Col materials supported a significantly larger load before rupturing compared to standard collagen vitrigels, suggesting that they can bear interrupted suture in clinical practice (Figure 1f).

As type I collagen concentrations gradually increase during vitrification of gels, collagen molecules self-assemble and eventually reach a nematic, liquid crystal-like structure.[23] Incorporation of CD into the collagen gelation and vitrification process interfered with the self-assembly process (Figure 2a). We found that the collagen fiber diameter, orientation, and lamella development depended on the size and chemical functionality of CD combined

with the gels (Figure 2b and Figure S1b,c, Supporting Information). Collagen fibers ranged from minimally detectable in gels with αCD, βCD, and γCD, to moderately detectable in αCD-SH, αCD-$NH_2$,βCD-$C_4H_9$ and readily observable in transmission electron micrographs (TEMs) of Col, αCD-Suc, αCD-$PO_4$, and βCD-Suc. The fibers observed by scanning electron microscopy (SEM) were either randomly oriented (αCD-SH, αCD-$PO_4$, βCD-$C_4H_9$, αCD-$NH_2$) or aligned in parallel over large regions (αCD-Suc, βCD-Suc), similar to the native cornea. Finally, lamellae were grossly visible (Figure 1d) and were also observed in TEMs of βCD and βCD-Suc containing materials and ranged in thickness from 0.5 to 5 μm. Formulations synthesized with αCD-SH and αCD–$CH_3$ did not form structured materials that could be handled and those with αCD-$PO_4$ and αCD-$NH_2$ were completely opaque. The size, charges, and hydrophilicity (or hydrophobicity) of the different functional groups affect the solubility and hydrophilicity of CDs[37,38] (e.g., hydrophobic–$C_4H_9$ and hydrophilic -succinyl), which in turn impact the interaction between the functionalized CDs and collagen during fibril assembly. The charges of the functional groups (e.g., –$NH_2$, –$PO_4$, and succinyl) may also cause nonspecific binding to the oppositely charged amino acids on the collagen chains. These complex interactions resulted in various ultrastructures within the collagen vitrigels (Figure S1b,c, Supporting Information). For further characterization, we selected the most representative formulations containing αCD, βCD, γCD, αCD-Suc, and βCD-Suc, which all produced transparent materials.

The size and functionality of the CD incorporated into the collagen gels impacted the bound water and thus water evaporation during the vitrification process. While all formulations started with similar liquid volumes and concentrations of collagen, the resulting CD/Col materials varied in water content (Figure S2a, Supporting Information), and thus collagen concentration (Figure S2b, Supporting Information) after vitrification. βCD/Col had the highest collagen concentration and lowest swelling ratio after vitrification, most similar to the native cornea. In contrast, αCD/Col and γCD/Col had the lowest collagen concentration and highest swelling ratio (Figure S2a,b, Supporting Information). This varying concentrating of collagen can influence the assembly through molecular crowding effects to produce unique ultrastructures.

Transparency is critical to the functionality of a cornea mimetic implant and is related to the collagen concentration and organization. Type I collagen-only materials (Col) without CD addition were prepared using the protocols for CD/Col vitrigel and served as controls. The Col materials used in this study were significantly different from CV, which contain cell culture media components and serum.[30] Col materials (without CD) had the lowest transparency values (Figure 2c). These implants were thin (≈150 μm) and were 88% transparent at 550 nm (average wavelength of white light) and only 62% when normalized to a 400 μm thickness. Therefore, achieving minimum functional transparency at a thickness of native human cornea would be impossible with these materials. Addition of βCD produced materials with the greatest transparency, 77% at 550 nm normalized to 400 μm (Figure 2c). No statistical significance was observed between the transparency of materials with different CD molecules (Figure 2c and Figure S2c,d, Supporting Information).

To further evaluate the physical properties resulting from the addition of CD to collagen vitrigel, we characterized the mechanical properties using multiple methods. The corneas are subjected to shear and tensile mechanical forces in vivo due to blinking and the intraocular pressures. Moreover, surgical implantation of a cornea substitute requires both elasticity and tensile strength to place and hold sutures like native tissue. Elasticity provides flexibility during the suturing process and prevents cracking from brittleness. Therefore, we tested and compared tensile, rheological (viscoelasticity), and compression properties of the implants with CD compared to collagen alone and the native cornea. The Young's modulus (stress/strain) was greatest for the collagen gel. However, the strain at fracture was the lowest of all of the groups (Figure 2d and Figure S2e,f, Supporting Information). This fracture at lower strain suggests lower suture hold strength. Implants containing βCD had a similar Young's modulus compared to the native cornea. The native cornea had a greater fracture strain compared to the βCD, but the difference was not significant. Cornea and βCD/Col both demonstrated significantly lower Young's modulus and higher strain at break than Col materials. Viscoelastic properties of the materials, measured by rheology, were significantly different between the groups and did not follow the same trends as the tensile properties. The βCD/Col materials had the greatest storage modulus, or in other words they exhibited the ability to store a higher quantity of deformation energy elastically (Figure 2e and Figure S2g, Supporting Information). The tan δ (ratio of loss modulus and storage modulus) of βCD/Col and the cornea were similar with no statistical difference. Thus, the βCD/Col materials exhibited tensile properties that would support suturing, and cornea-like viscoelastic properties.

To further compare the bulk properties of the CD/Col materials with the native cornea, we evaluated the denaturation temperature using differential scanning calorimetry (DSC). The specific heat required to denature βCD/Col and the native cornea were similar and significantly greater than all of the other formulations (Figure 2f and Figure S2h, Supporting Information). The higher value of denaturation temperature correlates with greater interfibrillar interactions between the collagen fibrils. Taken together, these morphological, mechanical, and functional data suggest that βCD/Col materials provide the best mimic of the native cornea and satisfy the design criteria of transparency and mechanical integrity required for a cornea substitute.

### 2.2. βCD Molecular Interactions Modulate Collagen Assembly

The bulk properties of the βCD/Col materials suggested a molecular interaction between the CD and collagen molecules that impacted assembly during gelation and/or assembly during vitrification. To explore the mechanisms of these interactions, we first considered the impact of CD on collagen secondary structure and fibril formation using circular dichroism. The typical collagen triple helix signal in circular dichroism over the wavelength spectrum has a positive band at 222 nm and a negative band at 200 nm.[39] Addition of CD to a collagen solution increased the temperature required to induce protein triple helix unfolding and denaturation as measured at 222 nm (Figure 3a, and Figure S3a, Supporting Information). This result implies increased stability of the collagen triple helix in the presence of CD molecules. Further, the addition of CD changed the characteristic collagen triple helix curve that is a strong negative peak at 200 nm (Figure 3b and Figure S3b, Supporting

Information). As collagen gelation occurs with neutralization, the characteristic collagen triple helix signal from circular dichroism is attenuated as the helices combine to form larger fibrils. Addition of CD reduced this signal attenuation, suggesting a direct molecular interaction that suppressed fibril formation and resulted in a limited fibril growth. Collagen fibrils observed in the SEM and TEM images further supported this mechanism.

To determine potential specific interactions between the CDs and collagen molecules, we evaluated the UV absorbance of collagen solutions with αCD, βCD, γCD, and βCD-Suc (Figure 3c and Figure S3, Supporting Information). βCD is known to bind with polypeptides containing aromatic groups[40,41] such as tyrosine,[42] as measured by a shift in wavelength or increase in absorbance at the characteristic tyrosine peak at 275 nm. Collagen was combined with the CDs at pH 3 in $1 \times 10^{-3}$ m HCl solution to avoid gelation, and the potential interactions of CD with collagen could be isolated. The UV– vis absorbance profile of collagen increased with the addition of CD, with βCD inducing the highest increase of absorbance (Figure 3c and Figure S3c, Supporting Information). This result confirmed that the CD molecules interact with the aromatic amino acids in collagen, especially tyrosine.

CD/collagen binding was further confirmed using quartz crystal microbalance (QCM). Collagen was deposited on a gold substrate after which a solution of CD was introduced (dotted line A, Figure 3d). The resonance frequency of the crystal changes when the mass of the coating changes, in this case when CD binds to collagen. Both βCD and βCD-Suc induced a frequency change in contrast to a control sucrose solution that cannot bind to collagen. When the CD solution was replaced by buffer (dotted line B, Figure 3d), the frequency partially and then completely returns to the initial levels for the βCD-Suc and βCD suggesting a reversible interaction. The reversibility of the CD/collagen interaction was further investigated by evaluating the presence of CD after vitrification and rehydration. When CD/Col materials were rehydrated after vitrification, an initial burst release of excess CD was observed followed by slow release of more closely bound CD that leached out over 48 h (Figure S3d, Supporting Information).

Due to the hydrophobic-core hydrophilic-shell nature of CD, upon reaching a certain concentration, CD itself will form aggregates.[43] Atomic force microscopy (AFM) allowed the observation of the CD aggregates in vitrified materials. The CD aggregates were visible at dry state right after vitrification in the phase shift channel and were always present close to collagen fibrils (Figure S4, Supporting Information, dry state). When the samples were rehydrated and dried again, the aggregates were no longer detectable (Figure S4, Supporting Information, rehydrated and dried state). Thus, these aggregates are likely formed by excess CD during the vitrification process. CD aggregations may contribute to the lamellae formation observed in the CD/Col materials after vitrification.

The strength of the collagen interaction with βCD was quantified by isothermal titration calorimetry (ITC). βCD forms aggregates at concentrations higher than $2–3 \times 10^{-3}$ m in neutral and acidic solutions,[44,45] and titration of a concentrated βCD solution at $13.2 \times 10^{-3}$ into $1 \times 10^{-3}$ m HCl solution presented a heat of dilution curve typically seen in an aggregate–monomer dissociation model. βCD ($13.2 \times 10^{-3}$ m) was then titrated against a 1 mg $mL^{-1}$ collagen solution in $1 \times 10^{-3}$ m HCl. Large exothermic peaks indicate that CDs

bind to the collagen and the attenuation of the endothermic peaks from control conditions ($1 \times 10^{-3}$ m HCl, no collagen) confirm that the βCD aggregate equilibrium shifts in favor of dissociation, and interaction with collagen (Figure 3e). The simulated binding affinity was calculated to be $511 \pm 27.4$ $m^{-1}$, giving a dissociation constant of $1.96 + 0.10 \times 10^{-3}$ m. The approximate number of binding sites was $10 \pm 3$ per collagen molecule, below the estimated number of aromatic amino acids in collagen.[46]

Taken together, the characterization of bulk properties and molecular interactions found that βCD binds with tyrosine and other hydrophobic amino acids on collagen with a dissociation constant of $1.96 + 0.10 \times 10^{-3}$ m (Figure 3f). This interaction leads to a reduced fibril diameter during gelation. In βCD-Suc, hydrophilic succinyl groups may interfere with the hydrophobic interactions between the aromatic groups on collagen and the CD inner core (Figure 3g). The succinyl groups may also potentially interact with positively charged amino acids, or form hydrogen bonds with other amino acids. The concentration of collagen during vitrification creates a liquid-crystalline phase allowing the formation of lamellae that was initiated by excess CD aggregates. The binding of CD to collagen is reversible, and therefore, the majority of the CD molecules can be removed after assembly. The resulting βCD/Col has local fibril alignment and organized lamellae that provide increased mechanical strength and transparency, with many similarities to the native cornea.

### 2.3. βCD/Col Biomimetic Cornea Biocompatibility and Surgical Performance

We evaluated corneal epithelial cell proliferation and biocompatibility on CD/Col implants through ex vivo and in vivo studies to demonstrate the functional and regenerative capacity of biomimetic CD/Col implants to wounded corneas.

Biocompatibility of the CD/Col implants was evaluated by in vitro epithelial cell culture and cornea explant culture to evaluate epithelial cell migration (Figure 4). Primary rabbit corneal epithelial cells seeded in vitro over CD/Col materials and reached confluence in 3–4 d. Keratin 14 (K14, epithelial cytoskeleton protein) staining revealed that primary corneal epithelial cells maintained epithelial morphology on all materials and expressed limbal stem cell-specific protein p63 (Figure S5a–g, Supporting Information). Gene expression for p63 (limbal epithelial stem cell marker), Connexin 43 (CX43, gap-junction protein), and Keratin 3 (K3, corneal epithelium specific cytokeratin protein) were evaluated to determine maturity of corneal epithelial cells (Figure S5h, Supporting Information). Epithelial cells on βCD/Col vitrigel expressed significantly higher expression of K3 compared to Col vitrigels. Concurrently, epithelial cells on βCD-Suc Col vitrigel presented significantly higher expressions of p63 and CX43, indicating maintenance of healthy epithelial cell phenotype and stem cell niche on CD/Col materials.

Epithelialization remains a significant challenge for corneal implants. We assessed migration and maturation of epithelial cells on CD/Col implants using an ex vivo corneal explant culture model (Figure 4a), to ensure that CD/Col materials support cell growth without the use of exogenous cells. Re-epithelialization completed at 72 h of culture, characterized by fluorescein staining (Figure 4b). Histological analysis at 72 h (Figure 4c) demonstrated epithelial cell coverage over the implant region. K14 was detected using

immunofluorescence (Figure 4d) in the epithelial cells, which migrated over the implant, indicating cell maturation and stability.

To translate the βCD/Col materials in vivo, curved implants were engineered to fit the anterior corneal surface. Custom-designed plastic molds were used (Figure 4e) to create lenticular implants (Figure 4f). Manufacturing protocols were developed that supported homogenous mixing of the CD and collagen along with vitrification in the custom molds. Resulting βCD/Col materials were implanted in a partial keratectomy corneal defect surgically created in a rabbit model (6 mm diameter, 150 μm depth, $n = 4$) (Figure 4g). The βCD/Col implants were sufficiently strong to be held in place using simple interrupted sutures. Re-epithelialization across the implant and integration with the adjacent host corneal tissue was followed over 31 d (Figure 4h–j and Figure S6, Supporting Information). Progress of epithelial cell migration was observed using fluorescein staining on the ocular surface (Figure 4j and Figure S6, Supporting Information). Epithelial defects, observed as fluorescent regions, decreased over time. Sutures were removed on day 21 postsurgery, by which time the implant had successfully integrated with surrounding tissue. Over 90% re-epithelialization was achieved by the last time point for the animal study. Masson's trichrome histological staining of the excised rabbit corneas at day 14 (Figure 4k) and day 31 (Figure S6, Supporting Information) demonstrated the presence of the implant and epithelial cell coverage over the βCD/Col material. Further, laminin proteins were expressed by migrated epithelial cells, indicating basement membrane formation on top of the implant (Figure 4l).

In conclusion, we engineered transparent and mechanically robust corneal substitutes by using cyclodextrins to modulate type I collagen self-assembly process during vitrification. These corneal substitutes have a unique ultrastructure that is similar to the native cornea. Mechanistic studies revealed that the CD molecules inhibited fibril formation and modulated lamellar formation organization, such that smaller fibers and lamellar structures were formed to increase transparency. The ability to suture the βCD/Col material, and its support of re-epithelialization and host tissue integration, demonstrates its potential as a biomimetic corneal substitute.

## 3. Experimental Section

### Synthesis of CD/Col Corneal Implants via Vitrification:

Equal volumes of 5 mg $mL^{-1}$ pH 3 solubilized Type I collagen solution (Cosmo Bio KOU-IPC-50) and 2.5 mg $mL^{-1}$ CD (Sigma Aldrich) solution, containing $20 \times 10^{-3}$ m HEPES (Lift Technologies) buffer at pH 11 were mixed at 4 °C and poured into hydrophilic culture dishes. The solution was then incubated at 37 °C and 5% $CO_2$ for 2 h to complete gelation. The resulting gel was then placed in a sterile humidifying chamber (vitrifier) at 5 °C and 40% relative humidity (RH) for 1 d. Gels were further dehydrated in a second vitrifier at 40 °C and 40% RH for 1 week to form transparent, rigid vitrigel materials. The resultant vitrigel materials were rehydrated in PBS overnight to form transparent, flexible, robust hydrogels prior to characterization, cell culture, or in vivo application.

### Electron Microscopy (EM):

Samples were fixed in 0.1 m sodium cacodylate buffer with 3% paraformaldehyde (PFA), 1.5% glutaraldehyde, 2.5% sucrose, and 0.1% tannic acid, then post-fixed in osmium tetroxide. The collagen fibrils were stained with aqueous uranyl acetate, dehydrated using a graded series of ethanol, and embedded in Eponate 12 resin (Ted Pella, Redding, CA). Thin sections, 60–90 nm were placed on naked copper grids then stained with uranyl acetate and lead. Images were taken by Philips CM120 TEM at 80 kV. SEM samples were fixed as described above and affixed to SEM stubs. A Leo FESEM was used to observe the samples. Lamellar thickness was determined using Image-J software on the TEM and SEM photomicrographs.

### Physical Characteristics Measurements:

Transparency was measured by placing fully rehydrated materials on 24-well plates, using the area scanning modality on a Biotek Synergy 2 microplate reader in the visible light wavelength range of 300–700 nm with 50 nm intervals.

Tensile testing was performed on hydrated materials using dog-bone shaped tensile test strips, each 5 mm in width. Digital Vernier calipers were used to measure the individual thickness of the CD/Col materials between two glass slides. Thickness was measured at six different points for each sample. CD/Col materials were then loaded onto a Bose EnduraTec (Minnetonka, MN) mechanical tester and stretched at a speed of 0.02 mm $s^{-1}$. Load versus displacement values were obtained, and fracture strain was recorded.

Rheology was performed with an Ares G2 rheometer (TA Instruments New Castle, DE). Experiments were conducted at physiological temperatures (37 °C). Samples of 8 mm diameter and 500 μm thickness were loaded on the rheometer stage and axial force was set to 1 N. The experimental design followed a frequency sweep from 0.1 to 100 Hz (2% strain), strain sweep from 1% to 100% (2 Hz frequency), oscillation time (5 min, 2 Hz, 2% shear). Three samples per group, per experiment, were tested under the same rheological protocol. Sample hydration was maintained using a solvent trap.

DSC was performed using a DSC 8000 (Perkin Elmer, Waltham, MA) to determine the denaturation temperature of the cornea and CD/Col materials. Preweighed hydrated samples were prepared and placed in aluminum sample pans and crimp-sealed with aluminum lids supplied by the manufacturer. Temperature ramp of 5 °C $min^{-1}$ over a range of 10 °C to 90 °C was run. DSC thermograms were analyzed using PyrisSeries Thermal Analysis software (Perkin Elmer) version 10.1.

### Biophysical Studies on the Mechanism of CD/Collagen Binding and Ultrastructure Formation:

UV/Vis absorption was measured by mixing CDs at 0.5 mg $mL^{-1}$ in 1 mg $mL^{-1}$ HCl acidic collagen solution at pH 3. Following mixing, solution was degassed and 1 mL of each solution was pipetted into wells of 24 well plates and Biotek Synergy 2 microplate reader was used to measure absorbance of wavelengths in the 250–300 nm range.

Circular dichroism spectra of collagen solution at 0.125 mg $mL^{-1}$ at pH 3, over the range 190–250 nm were obtained using Aviv Biomedical spectrometer. Collagen was brought to pH 7 using $20 \times 10^{-3}$ m HEPES buffer, with or without the presence of CDs at 0.0625 mg $mL^{-1}$. Circular dichroism was recorded at 222 nm (absorption bands of the collagen triple helix) for different solutions over a temperature gradient of 30 to 60 °C.

A quartz-crystal microbalance (QCM, Qsense E4, Biolin Scientific Inc, Glen Burnie MD) was used to detect binding of CDs onto a physisorbed collagen surface. Collagen at 1 mg $mL^{-1}$ in $1 \times 10^{-3}$ m HCl was adsorbed over pristine gold surface until saturation. Following this, a stable baseline was acquired with $1 \times 10^{-3}$ m HCl flow, without collagen. Then, CDs dissolved in $1 \times 10^{-3}$ m HCl at a concentration of $0.44 \times 10^{-3}$ m and passed through a 0.22 μm filter, were pumped at flow rate of 0.05 mL $min^{-1}$ through the measurement chambers. Following signal stabilization, pure $1 \times 10^{-3}$ m HCl was flowed through the chambers again. The instrument was used to record changes in resonance frequency (fundamental resonance frequency was 5 MHz, overtones recorded were $n = 3, 5, 7, 9, 11$).

To quantify the βCD binding affinity to collagen molecules, isothermal titration calorimetry (ITC) was used. Collagen (5 mg $mL^{-1}$) was dialyzed in 3 L of $1 \times 10^{-3}$ m HCl buffer for 24 h and diluted to 1 mg $mL^{-1}$ with the dialysis buffer. Concentrated βCD at $13.2 \times 10^{-3}$ m was prepared using the same dialysis buffer. All binding parameters were measured at 20 °C using 1.4 mL of 1 mg $mL^{-1}$ collagen sample in the cell titrated with 25 injections 10 μL βCD solution each. The sample and reference cells were cleaned extensively before each run. The isothermal curve was obtained by integration of individual peaks and after subtracting the average heat of dilution. Binding parameters were determined from titration binding curves using the one site model from the software MicroCal Data Analysis (Malvern, Westborough, MA).

### Ex Vivo Cell Migration:

Fresh rabbit eyes were purchase from PelFreez. Implants of 6 mm diameter were surgically inserted into an ex vivo cornea after creation of a partial pocket model with a 4 mm anterior wound (Figure 4a). The corneas with the implants were placed on contact lens mold, then air-lift cultured in full media (DMEM + 10% FBS) up to 72 h. Reepithelialization was tracked using Fluoresoft solution. At harvest, some samples were fixed in 10% formalin and embedded in paraffin for standard histology, and some inserted implants were careful removed and fixed in 4% PFA for immunofluorescent staining. Primary antibody mouse anti-human K14 and secondary antibody AlexaFluor562 goat antimouse IgG (Life Technologies) were stained on the implants, followed by counterstaining of DAPI. Samples were observed and imaged with Inverted Fluorescent scope (Zeiss).

### In Vivo Surgical Procedures and Postoperative Care:

All experimental procedures in this study were performed in accordance to the Association for Research in Vision and Ophthalmology Statement for the Use of Animals in Ophthalmic and Visual Research and were approved by the Institutional Animal Care and Use Committee at Johns Hopkins University. Anterior lamellar keratectomy was performed on male New Zealand albino rabbits (weight: 2.5–3.5 kg) under anesthesia by intramuscular

administration of ketamine (35 mg $kg^{-1}$) and xylazine (5 mg $kg^{-1}$). Proparacaine (Akorn, Lake Forest, IL) was administered on the corneal surface prior to the surgical procedure. A 6 mm Hessburg-Barron vacuum trephine (Barron Precision Instruments LLC, Grand Blanc, MI) and a crescent knife (LaserEdge, Bausch&Lomb, Rochester, NY) were used to remove approximately 150 μm of anterior corneal tissue. βCD/Col corneal substitutes (approximately 125 μm thickness, 6.25 mm diameter and 7.5 mm curvature) were implanted using 12–14 interrupted 10–0 nylon sutures. PRED-G ointment (Allergan, Irvine, CA) was applied for 14 d as a postoperative treatment. Gross observations, including ophthalmomicroscopy and fluorescein staining, were performed at day 3, 7, 14, 21, and 31 d after surgery. All animals received the same treatment. Therefore, no randomization was used to determine implant survival in rabbits. Consequently, researchers were not blinded. Corneas were harvested at 31 d postsurgery, fixed in formalin and processed for histology. Sections on slides were then processed for standard histological hematoxylin and eosin (H&E) staining, Masson's Trichrome staining, and for immunohistochemical staining of laminin.

### Statistical Analysis:

All experimental analyses were performed samples of at least $n = 3$, representative of two or more independent studies. No statistical method was used to predetermine sample size in animals. Data were expressed as mean ± standard deviation and statistical significance ($p$ value) between conditions was determined by one-way analysis of variance (ANOVA) with the Bonferroni post hoc test using GraphPad Prism 5.

### Data Availability:

The data that support the findings of this study are available upon reasonable request from the corresponding author.

## Supplementary Material

Refer to Web version on PubMed Central for supplementary material.

## Acknowledgements

S.M. and X.W. contributed equally to this work. This research was supported by our sponsors Research to Prevent Blindness, National Eye Institute grant R01EY029055, Eyegenix LLC (Prime Sponsors US Department of Defense and US Army Medical Research and Material Command) and the Morton Goldberg Professorship. The authors thank our colleagues from Eyegenix LLC, Honolulu (Tony Lee, Derek Duan, Priscilla Carbajal, Jack England, and Kylie Matsumoto) for helpful discussions. We would also like to acknowledge Scot C. Kuo (Director), Michael Delannoy (Associate Director) and Barbara Smith (EM & Advanced Fluorescence Microscopy Specialist) at the Microscopy Facility at Johns Hopkins School of Medicine, and EY001765 Wilmer Core Grant for Vision Research, Microscopy and Imaging Core Module. The authors also thank Katherine Tripp (Center Manager) at the Center for Molecular Biophysics for her advice and training on the circular dichroism spectrometer. The authors acknowledge Archana Jaiswal (Principal Application Scientist) at Biolin Scientific for training and use of the QSense QCM-D machine. Further, the authors acknowledge Harry Saaverdra Espinoza, Postdoctoral Fellow in the Amzel Lab in Johns Hopkins School of Medicine for assistance with the ITC experiments. The authors also extend thanks to Caitlin Duckwall and Dhruv Majumdar for the digital illustrations.

## References


[1]. Di Lullo GA, Sweeney SM, Korkko J, Ala-Kokko L, San Antonio JD, J. Biol. Chem2002, 277, 4223. [PubMed: 11704682]

[2]. Tocce EJ, Smirnov VK, Kibalov DS, Liliensiek SJ, Murphy CJ, Nealey PF, Biomaterials2010, 31, 4064. [PubMed: 20153044]

[3]. Gasiorowski JZ, Murphy CJ, Nealey PF, Annu. Rev. Biomed. Eng2013, 15, 155. [PubMed: 23862676]

[4]. Raghunathan V, McKee C, Cheung W, Naik R, Nealey PF, Russell P, Murphy CJ, Tissue Eng., Part A2013, 19, 1713. [PubMed: 23488816]

[5]. Freund DE, McCally RL, Farrell RA, Cristol SM, L'Hernault NL, Edelhauser HF, Invest. Ophthalmol. Visual Sci1995, 36, 1508. [PubMed: 7601631]

[6]. Bron AJ, Br. J. Ophthalmol2001, 85, 379. [PubMed: 11264120]

[7]. Komai Y, Ushiki T, Invest. Ophthalmol. Visual Sci1991, 32, 2244. [PubMed: 2071337]

[8]. Holmes DF, Gilpin CJ, Baldock C, Ziese U, Koster AJ, Kadler KE, Proc. Natl. Acad. Sci. USA2001, 98, 7307. [PubMed: 11390960]

[9]. Meek KM, Quantock AJ, Prog. Retinal Eye Res2001, 20, 95.

[10]. Zhang G, Chen S, Goldoni S, Calder BW, Simpson HC, Owens RT, McQuillan DJ, Young MF, Iozzo RV, Birk DE, J. Biol. Chem2009, 284, 8888. [PubMed: 19136671]

[11]. Chen S, Mienaltowski MJ, Birk DE, Exp. Eye Res2015, 133, 69. [PubMed: 25819456]

[12]. Stamov DR, Muller A, Wegrowski Y, Brezillon S, Franz CM, J. Struct. Biol2013, 183, 394. [PubMed: 23747391]

[13]. Qazi Y, Hamrah P, J. Clin. Cell. Immunol2013, Suppl 9: 6, 10.4172/2155-9899.S9-006.

[14]. Niederkorn JY, Curr. Opin. Allergy Clin. Immunol2010, 10, 493. [PubMed: 20689406]

[15]. Fink N, Stark WJ, Maguire MG, Stulting D, Meyer R, Foulks G, Smith RE, Rapoza P, Cesk. Oftalmol1994, 50, 3. [PubMed: 8137435]

[16]. Maguire MG, Stark WJ, Gottsch JD, Stulting RD, Sugar A, Fink NE, Schwartz A, Ophthalmology1994, 101, 1536. [PubMed: 8090456]

[17]. Jiraskova N, Rozsival P, Burova M, Kalfertova M, Eye2011, 25, 1138. [PubMed: 21681219]

[18]. Ahn JI, Kuffova L, Merrett K, Mitra D, Forrester JV, Li F, Griffith M, Acta Biomater. 2013, 9, 7796. [PubMed: 23619290]

[19]. Alarcon EI, Udekwu K, Skog M, Pacioni NL, Stamplecoskie KG, Gonzalez-Bejar M, Polisetti N, Wickham A, Richter-Dahlfors A, Griffith M, Scaiano JC, Biomaterials2012, 33, 4947. [PubMed: 22494887]

[20]. Alarcon EI, Udekwu KI, Noel CW, Gagnon LB, Taylor PK, Vulesevic B, Simpson MJ, Gkotzis S, Islam MM, Lee CJ, Richter-Dahlfors A, Mah TF, Suuronen EJ, Scaiano JC, Griffith M, Nanoscale2015, 7, 18789. [PubMed: 26507748]

[21]. Fagerholm P, Lagali NS, Merrett K, Jackson WB, Munger R, Liu Y, Polarek JW, Soderqvist M, Griffith M, Sci. Transl. Med2010, 2, 46ra61.

[22]. Fagerholm P, Lagali NS, Ong JA, Merrett K, Jackson WB, Polarek JW, Suuronen EJ, Liu Y, Brunette I, Griffith M, Biomaterials2014, 35, 2420. [PubMed: 24374070]

[23]. Tidu A, Ghoubay-Benallaoua D, Lynch B, Haye B, Illoul C, Allain JM, Borderie VM, Mosser G, Acta Biomater. 2015, 22, 50. [PubMed: 25931016]

[24]. De Sa Peixoto P, Deniset-Besseau A, Schmutz M, Anglo A, Illoul C, Schanne-Klein M-C, Mosser G, Soft Matter2013, 9, 11241.

[25]. Saeidi N, Karmelek KP, Paten JA, Zareian R, DiMasi E, Ruberti JW, Biomaterials2012, 33, 7366. [PubMed: 22846420]

[26]. O'Leary LE, Fallas JA, Bakota EL, Kang MK, Hartgerink JD, Nat. Chem2011, 3, 821. [PubMed: 21941256]

[27]. Dewavrin JY, Hamzavi N, Shim VP, Raghunath M, Acta Biomater. 2014, 10, 4351. [PubMed: 24932771]

[28]. Chellam J, Mandal AB, Int. J. Pharma Bio Sci2013, 4, 795.

[29]. Takezawa T, Ozaki K, Nitani A, Takabayashi C, Shimo-Oka T, Cell Transplant. 2004, 13, 463. [PubMed: 15468688]

[30]. McIntosh Ambrose W, Salahuddin A, So S, Ng S, Ponce Marquez S, Takezawa T, Schein O, Elisseeff J, J. Biomed. Mater. Res., Part B2009, 90, 818.

[31]. McIntosh Ambrose W, Schein O, Elisseeff J, Curr. Stem Cell Res. Ther2010, 5, 37. [PubMed: 19951256]

[32]. Calderon-Colon X, Xia Z, Breidenich JL, Mulreany DG, Guo Q, Uy OM, Tiffany JE, Freund DE, McCally RL, Schein OD, Elisseeff JH, Trexler MM, Biomaterials2012, 33, 8286. [PubMed: 22920579]

[33]. Majumdar S, Guo Q, Garza-Madrid M, Calderon-Colon X, Duan D, Carbajal P, Schein O, Trexler M, Elisseeff J, J. Biomed. Mater. Res., Part B2016, 104, 300.

[34]. Saenger W, Biochem. Soc. Trans1983, 11, 136.

[35]. Guo Q, Phillip JM, Majumdar S, Wu PH, Chen J, CalderonColon X, Schein O, Smith BJ, Trexler MM, Wirtz D, Elisseeff JH, Biomaterials2013, 34, 9365. [PubMed: 24041426]

[36]. Chae JJ, Ambrose WM, Espinoza FA, Mulreany DG, Ng S, Takezawa T, Trexler MM, Schein OD, Chuck RS, Elisseeff JH, Acta Ophthalmol. 2015, 93, e57. [PubMed: 25495158]

[37]. Kraus T, Budesinsky M, Zavada J, J. Org. Chem2001, 66, 4595. [PubMed: 11421779]

[38]. Khuntawee W, Karttunen M, Wong-Ekkabut J, Phys. Chem. Chem. Phys2017, 19, 24219. [PubMed: 28848954]

[39]. Greenfield NJ, Nat. Protoc2006, 1, 2876. [PubMed: 17406547]

[40]. Yeguas V, Altarsha M, Monard G, Lopez R, Ruiz-Lopez MF, J. Phys. Chem. A2011, 115, 11810. [PubMed: 21913730]

[41]. Aachmann FL, Otzen DE, Larsen KL, Wimmer R, Protein Eng. 2003, 16, 905. [PubMed: 14983070]

[42]. Shanmugam M, Ramesh D, Nagalakshmi V, Kavitha R, Rajamohan R, Stalin T, Spectrochim. Acta, Part A2008, 71, 125.

[43]. Petitjean L, Reffay M, Grasland-Mongrain E, Poujade M, Ladoux B, Buguin A, Silberzan P, Biophys. J2010, 98, 1790. [PubMed: 20441742]

[44]. Messner M, Kurkov SV, Jansook P, Loftsson T, Int. J. Pharm2010, 387, 199. [PubMed: 19963052]

[45]. He Y, Fu P, Shen X, Gao H, Micron2008, 39, 495. [PubMed: 17706427]

[46]. Takaoka K, Koezuka M, Nakahara H, J. Orthop. Res1991, 9, 902. [PubMed: 1919854]

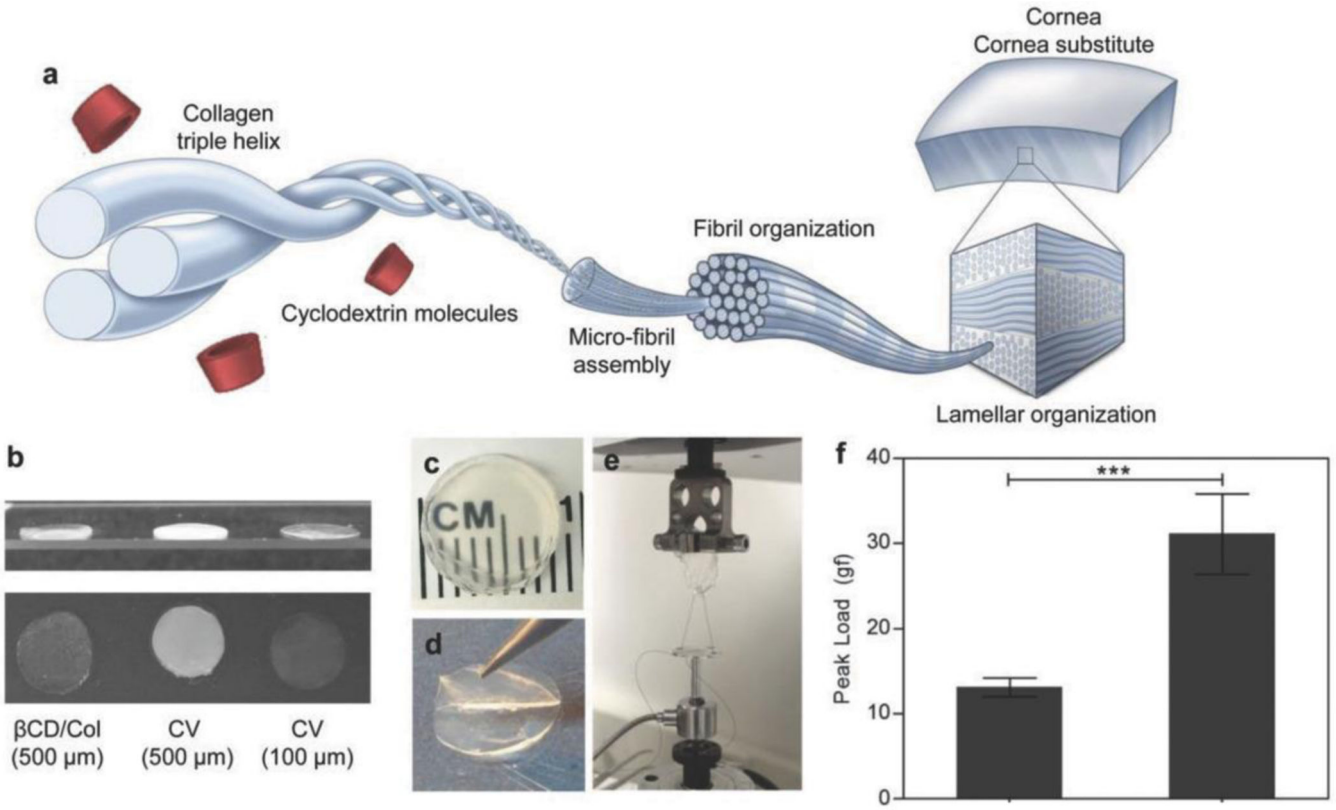


**Figure 1.**

Cyclodextrins modulate fibril formation and alignment in vitrified collagen cornea substitutes via interactions with collagen. a) Schematic demonstrating cyclodextrin–collagen interaction, ultimately influencing collagen ultrastructural organization and spacing. b) Gross comparison of CD/ Col materials with CV of different thicknesses. c) Gross image of 500 μm thickness implants manufactured using βCD-Suc and collagen to demonstrate optical clarity. d) Evidence of macroscale lamellar structures in the implants as evidenced by careful peeling of individual layers. e) Suture pullout testing set-up to measure suture retention of biomaterials. f) Peak load measurements to monitor suture retention strength of vitrigels (n = 6). Data are means ± SD, unpaired Student's t-test, ***P < 0.0001

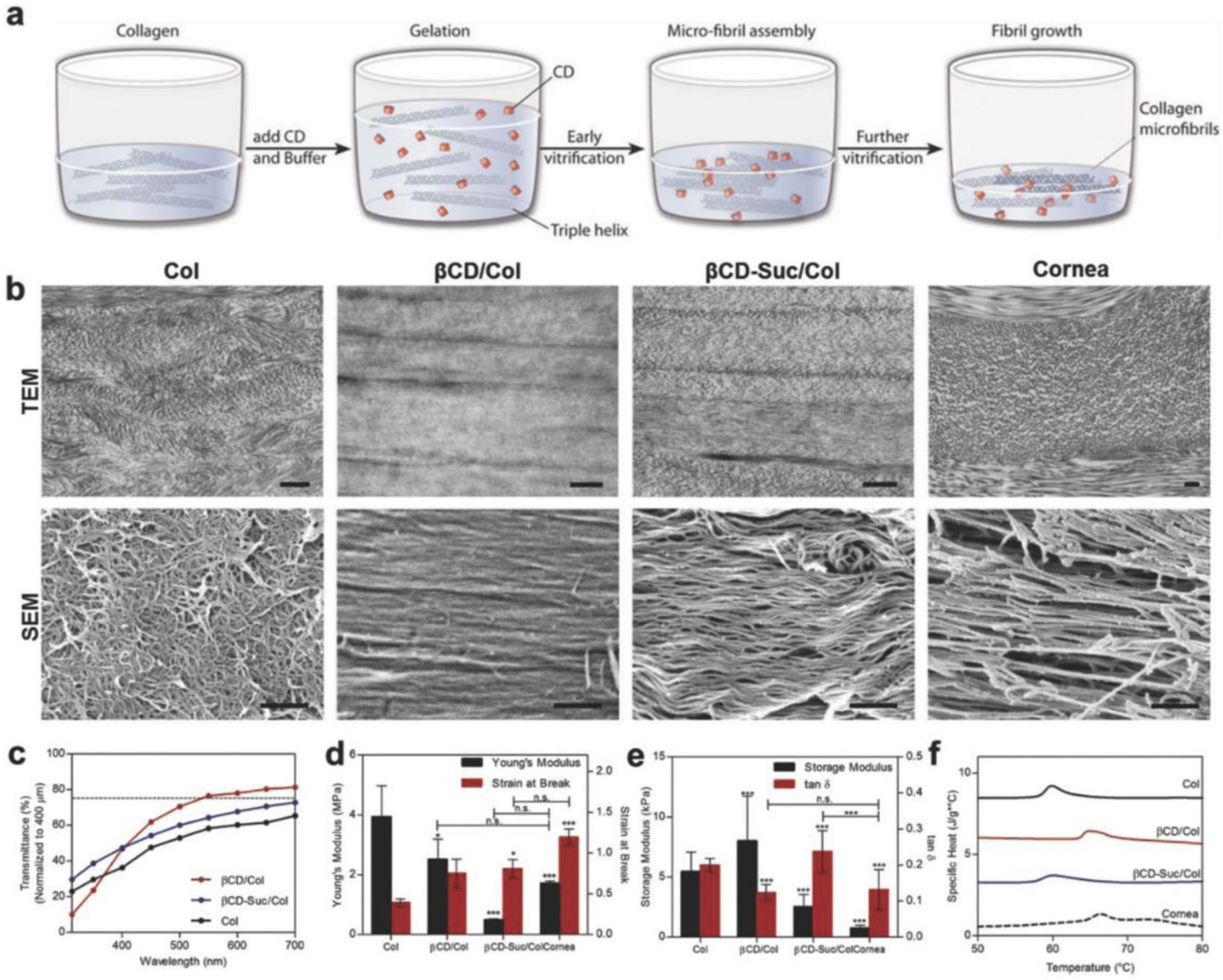


**Figure 2.**

Cyclodextrin functional groups define collagen fibril organization, transparency and mechanical properties. a) Vitrigels manufactured by mixing equal volumes of collagen and CD-buffered solution causing gelation and microfibrillar assembly followed by fibril growth and reorganization during controlled dehydration (vitrification). b) Transmission electron microscopy and scanning electron microscopy of Col, $\beta$CD, and $\beta$CD-Suc, and native rabbit cornea, to demonstrate effect of CD functionality on collagen ultrastructure organization. Scale bar = 500 nm. c) Light transmission over visible light spectrum of vitrigel formulations (normalized to 400 μm) with and without cyclodextrins, d) Young's modulus and strain at break measurements to monitor tensile properties of vitrigels following cyclodextrin incorporation. e) Oscillatory rheological properties of vitrigel formulations with cyclodextrin functionalization. f) Differential scanning calorimetry thermograms to determine thermal stability of vitrigels following incorporation of CD. Data are means ± SD, $n \geq 3$ (representative of at least two independent experiments), analysis of variance

(ANOVA) with Bonferroni's post-test: ***$P < 0.0001$, **$P < 0.001$, *$P < 0.01$ compared against Col unless otherwise specified.

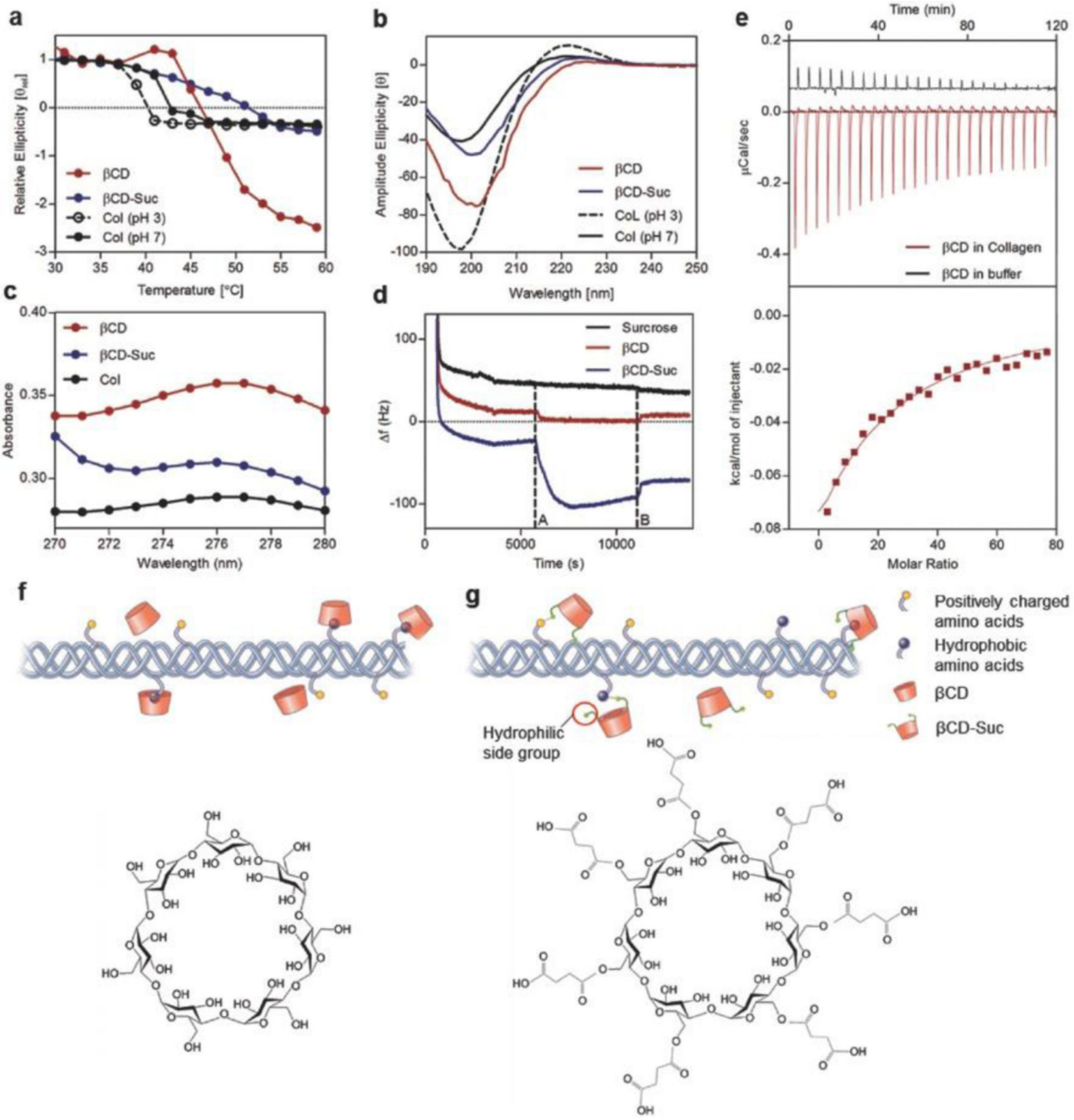


**Figure 3.**

Collagen–cyclodextrin molecular interactions and effect on fibril formation. a) Circular dichroism spectroscopy among groups to demonstrate changes in thermal stability following molecular interactions between soluble collagen and *β*CD, b) CD spectrum of collagen triple helix with and without CD at a temperature of 5 °C. c) Shift in UV–vis light spectrum absorbance peak following incorporation of *β*CD and *β*CD-Suc into soluble collagen. d) Frequency change associated with *β*CD and *β*CD-Suc deposition and binding to collagen coated substrate via QCM analyses (frequency overtone $n = 5$). e) Quantification of binding

affinity of βCD with collagen via ITC at 20 °C. f) Schematic showing interaction of collagen hydrophobic groups with hydrophobic inner core of βCD and chemical structure. g) Incorporation of βCD-Suc in collagen involves additional interaction of the highly hydrophilic succinyl side chains and βCD-Suc chemical structure.

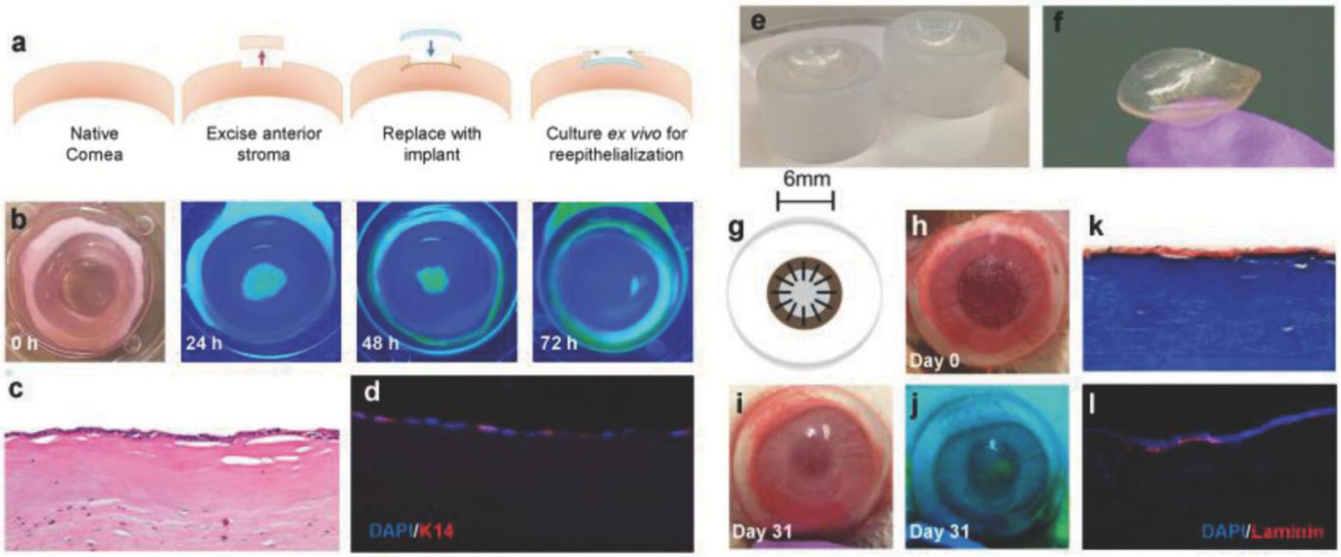


**Figure 4.**

Functional compatibility and surgical in vivo performance of biomimetic collagen-CD implants. a) Schematic outlining implantation of CD/ Col materials in ex vivo rabbit corneas. b) Progress of corneal epithelial wound healing over 72 h observed via fluorescein staining. Yellow-green staining under blue light indicates regions without epithelial cell coverage. c) Proliferation of epithelium observed across implants at 72 h using H&E histology. d) DAPI (blue) and K-14 (red) staining via immunohistochemistry of implanted ex vivo cornea sections to visualize cell maturation and functional epithelium. e) Custom molds used for manufacturing implants with desired curvature. f) Lenticularly shaped βCD/Col corneal implants with curvature of healthy cornea. g) Schematic of in vivo implantation of corneal implant and affixation using interrupted sutures. h) Gross image of the in vivo ocular surgery in the rabbit model on the day of surgery. i) Gross image of the in vivo ocular surface at 31 d. j) Fluorescein staining (under blue light) at day 31 to monitor progress of reepithelialization over βCD/Col implant. k) Histological analysis of sections stained using Masson's Trichrome to visualize implant after 14 d. l) Immunostaining for laminin (red) and DAPI (blue) in peripheral and central wound regions. Laminin proteins are expressed by epithelial cells after maturation.